Available online at www.sciencedirect.com
SCIENCE DIRECT®
Thin Solid Films 513 (2006) 289–294
thin solid films
www.elsevier.com/locate/tsf

Fabrication of densely packed, well-ordered, high-aspect-ratio silicon nanopillars over large areas using block copolymer lithography

Vignesh Gowrishankar [a], Nathaniel Miller [a], Michael D. McGehee [a,*], Matthew J. Misner [b], Du Yeol Ryu [b], Thomas P. Russell [b], Eric Drockenmuller [c], Craig J. Hawker [c]

[a] *Department of Materials Science and Engineering, Stanford University, Stanford, CA 94305-2205, USA*
[b] *Department of Polymer Science and Engineering, University of Massachusetts, Amherst, MA 01003, USA*
[c] *Materials Research Laboratory, University of California, Santa Barbara, CA 93106, USA*

Received 29 August 2005; received in revised form 22 December 2005; accepted 20 January 2006
Available online 3 March 2006

Abstract

The fabrication process for well-ordered nanopillars over large substrate areas, which are taller than 100 nm, have aspect ratios as high as 10 : 1 and occur with a periodicity of less than 35 nm is described. Various unique aspects of the materials and processing techniques enabled key features of the nanostructures: *block copolymer lithography* facilitated the small periodicity and the well-ordered arrangement of the pillars, a unique lift-off technique overcame potentially prohibitive lift-off problems, and a highly selective and anisotropic NF_3 based *reactive ion etching* achieved the final nanopillar structure. The specifics of the processing can be suitably modified to obtain pillars with different physical characteristics.

Keywords: Block-copolymer; Lithography; High-aspect-ratio; Lift-off; Nanopillars; Reactive ion etching

1. Introduction

Vertically oriented nanopillars and nanowires have sparked considerable interest in a variety of fields. In particular, sub-100 nm nanopillar periodicities are desirable for many applications, including bulk-heterojunction, organic–inorganic photovoltaic devices in which a ~150-nm-tall inorganic nanopillar network is infiltrated with a light-absorbing, organic semiconductor. If the pillar spacing could be controlled from 100 nm to less than 40 nm, this interpenetrating network of semiconductors would have the required absorption depth [1,2], favorable alignment of the organic semiconductor and exciton-splitting interfaces within 15 nm of all regions of the organic semiconductor [2]. In addition, two-dimensional photonic crystals and waveguides can be constructed using a structure of nanopillars of appropriate periodicity. A high refractive index material in the form of 200-nm-tall pillars arranged with a periodicity of 80 nm, for example, can be used for in-plane waveguiding sub-400 nm light [3,4]. Such a structure could be further integrated into a structure that simultaneously achieves out-of-plane waveguiding (via total-internal-reflection), thereby effecting a complete waveguide. Vertically oriented field-effect transistors, that permit decoupling of device density from channel length, may also be constructed using a similar nanopillar structure of an appropriate semiconductor [5]. In addition, nanopillar structures can also be used as stamps for nano-imprint lithography, providing a cheaper and faster alternative to the electron beam lithography route of manufacturing them. This paper describes the fabrication process for densely packed, well-ordered, high-aspect-ratio silicon nanopillars that can be patterned over large substrate areas using block copolymer (BCP) lithography and reactive ion etching (RIE). The materials and processes used on centimeter-sized substrates yield well-ordered nanopillars, which are taller than 100 nm, have aspect ratios as high as 10 : 1, and occur with a periodicity of less than 35 nm. We study the effect of different processing conditions on the physical structure of the pillars and the chemical composition of the pillar surface. The specifics of the processing can be suitably modified

* Corresponding author.
E-mail address: mmcgehee@stanford.edu (M.D. McGehee).

0040-6090/$ - see front matter © 2006 Elsevier B.V. All rights reserved.
doi:10.1016/j.tsf.2006.01.064

and we make suggestions on how to obtain pillars with different physical characteristics.

BCP lithography involves a self-assembly process that affords well-ordered patterns with periodicities ranging from 15 to 100 nm over large areas with relative ease and speed. It has been used previously to fabricate ordered arrays of Cr, Au/Cr and silicon oxide nanodots [6–8]. Chemically different block copolymers have also been used to pattern nanodimples in Ge and nanodots of GaAs [9,10], while magnetic dot arrays and silica posts have been fabricated using BCPs with an organometallic phase as one of the blocks [11–13]. BCPs have also been used to fabricate silicon nanopores, with a structure inverted in relation to the target of this work, and nanopillars, with lower aspect-ratio and wider spacing in relation to ours [14–16]. Nanosphere lithography and electron beam lithography are other available sub-100 nm patterning techniques, but neither allows for both well-ordered patterns and high throughput concomitantly.

The BCP pattern, once realized, must be transferred into the substrate. In conjunction with the BCP used, a metal etch-mask, obtained via lift-off, provides the appropriate patterning geometry to achieve the nanopillars. In order to fabricate high-aspect-ratio nanopillars, one must use a highly selective, anisotropic etch chemistry, a sufficiently thick etch-mask, or both. However, block copolymer lithography does not allow etch-masks thicker than 5–10 nm [8] to be deposited because of problems in the lift-off step. Furthermore, even with a very thin layer of the etch mask (under 5 nm), lift-off is not trivial and does not occur uniformly across the surface. We report a novel way to circumvent the lift-off problem as well as an uncommon RIE chemistry to achieve the desired nanostructures.

2. Experimental details

2.1. The fabrication of the block copolymer template

Templates for the fabrication of the nanopillars on Si wafers were made from diblock copolymers of poly(styrene-*b*-methylmethacrylate), PS-*b*-PMMA [6,17,18]. First, a 2 wt.% solution of a random copolymer of styrene and methylmethacrylate (styrene fraction of 0.58) was spin-coated on Si wafers at low speeds of ca. 1500 rpm. The Si was then heated to 175 °C in vacuum for 72 h to anchor the random copolymer to the native oxide layer. Excess copolymer was washed off using toluene and the remaining layer served to balance interfacial interactions between the blocks and the substrate. Onto this modified substrate, a 1 wt.% solution in toluene of the block copolymer (PS-*b*-PMMA, Mol. Wt. 88,000 g/mol, 70 vol.% polystyrene), was spin-coated at speeds between 3000 and 3500 rpm. The film thickness corresponded to one repeat period, or ca. 30 nm. Subsequent annealing in vacuum at 175 °C for 24 h produced a film with the cylindrical microdomains oriented normal to the surface. Templates using PS-*b*-PMMA of molecular weights 72,000 g/mol and 65,000 g/mol were also successfully fabricated.

Upon exposure to UV radiation (254 nm, 18 W/cm^2, for 35 min), the PMMA forming the cylindrical domains degraded and the PS matrix underwent crosslinking. The wafer was then rinsed in glacial acetic acid for 35 min, followed by a rinse in de-ionized water for 10 min. This resulted in a crosslinked film of PS having an array of hexagonally packed nanopores that spanned the film. A brief oxygen-plasma etch (100 sccm O_2, 26.66 Pa chamber pressure, 130 V bias voltage) cleared the Si surface of any remaining neutral underlayer and promoted the adhesion of the metal etch-mask.

2.2. Transferring the pattern into Si

Cr was found to be a suitable etch mask for the chosen RIE chemistry [19]. Between 2 and 5 nm of Cr was deposited at a rate of ca. 0.4 Å/s using an electron-beam evaporator (Innotec, at the Stanford Nanofabrication Facility). Conventional lift-off was attempted using procedures ranging in severity from soaking in toluene (for up to 24 h) to 2 h of sonication in toluene at 60 °C. These procedures were found to be ineffective in leaving only Cr islands over large areas of the Si by removing the BCP template.

This lift-off problem was circumvented by using an oblique-angled Ar sputter-etch by a system designed for depth-profiling experiments in an X-ray photoelectron spectroscopy setup (Leybold Hereaus Ar-ion gun). This was tailor-made for sequentially removing thin layers of material. A 10-mA-beam of Ar ions with an energy of 3000 eV and an incident angle of 35° (with the surface) was used to perform the sputter-etching. A discussion of the mechanism of this sputter-etching is presented in a later section. The area rastered by the ion-etch-gun was typically 0.5 × 0.5 cm, although larger areas were also successfully sputter-etched. Only certain sputter-etch-times yielded good nanostructures. Optimization of the sputter-etch time was done by sputter-etching samples for different times within a range dictated by the etch-rate of the sample in such a setup. The range in our case was between 1 and 18 min. We found, repeatedly, that 10 min of sputter-etching, with a window of leniency of about 2–3 min, gave the best nanostructures (after RIE).

The reactive ion etching was done using NF_3 gas (20 sccm NF_3, 2.66 Pa chamber pressure, 430 V bias voltage) [19] in the AMT 8100 Plasma Etcher (at the Stanford Nanofabrication Facility). This etch chemistry provided sufficient anisotropy and selectivity between the etch-mask and the substrate. The approximate Si etch rate of 25 nm/min was used to estimate etch times. RIE times between 3 and 8 min were tried.

2.3. Surface preparation of the nanopillars

Following the RIE, the Si nanopillars were subjected to UV-ozone treatment for about 60 min, which removed most of the C, N and F debris. Alternate immersion and rinsing in hydrofluoric acid (2 vol.% in water) and de-ionized water for ca. 15 min stripped the Si of the oxide and yielded chemically pristine Si nanopillars.

2.4. Characterization

The nanopillar structures were characterized by scanning electron microscopy (FEI XL30 Sirion SEM with a *field*

emission source) operated at an accelerating voltage of between 3 and 5 kV. Images of the nanopillars were typically taken at a tilt of 45°, which gave a better perspective of the structures. Other images of the block copolymer and Cr islands were also taken with the same SEM, but with no tilt.

The surface chemistry of the nanopillars was characterized using X-ray photoelectron spectroscopy (XPS, using an SSI S-Probe Spectrometer). Monochromatized Al(Kα) radiation (1486 eV) was used to probe the sample. The X-ray spot size was 250 × 1000 μm and the take-off angle of the detected electrons (with the sample surface) was 35°. With these conditions, the effective electron escape depth providing about 60% of the total signal, from a horizontal sample surface, would be ca. 12 Å The Ar ion-gun was part of this XPS setup.

3. Results and discussion

Once the block copolymer templates were obtained on the Si, a suitable etch-mask in conjunction with a selective RIE was needed to achieve the nanopillars. Finding such an etch chemistry that allowed the use of the BCP template directly as an etch-mask proved difficult (also, this would achieve nanopores and not nanopillars). Thus, a metal-deposition and lift-off of the BCP template was used. Cr was the metal of choice as the etch-mask during reactive ion etching (RIE), in part because it is extremely resistant to the NF_3 gas used for RIE, etching with a reported rate of about 0.5 nm/min, while Si is reported to etch at 30 nm/min when patterned at a lengthscale of hundreds of nanometers [19]. To achieve nanopillars taller than 100 nm, a 2-nm Cr etch-mask should meet the minimum requirement, but a few iterations of metal depositions and RIEs revealed that for a robust etch-mask, 5 nm of Cr was necessary. Conventional lift-off was attempted using procedures ranging in severity from dissolution in toluene to sonication in toluene at 60 °C. Fig. 1a shows a schematic of the (ideal) lift-off strategy used to produce islands of Cr etch-mask. However, even with just 2 nm of Cr, lift-off could not be achieved except over isolated domains a few microns across (Fig. 1b). Thicker masks of Cr only exacerbated this lift-off problem. With no evaporated Cr on them, the PS matrix readily dissolved after soaking for just 10 min in toluene, indicating that the PS is only partially crosslinked. During metal evaporation, sidewalls of Cr, which are probably thin and discontinuous, form on the insides of the cylindrical pores. However, these sidewalls of Cr effectively prevented the net dissolution of the templates, either by preventing sufficient penetration of solvent into the PS, or by impeding removal of chunks of crosslinked polymer through the discontinuous sidewalls, or both (Fig. 1c). The sporadic lift-off using Cr was unacceptable, especially for purposes of achieving large-area nanostructures. The deposition of different metals, such as Au and Al, was also examined and while these showed better lift-off properties, they proved ineffective as RIE etch-masks.

The lift-off problem was circumvented by using an oblique-angled Ar sputter-etch of the Cr-coated BCP template. Being obliquely incident, the Ar ions sputtered away the top surface and sidewalls of the Cr-coated PS, while leaving the islands of Cr on the silicon surface unharmed, as shown in Fig. 1c. The Ar ions must be incident obliquely since a vertical sputter-etch would sputter away the Cr islands on the Si, which serve as RIE etch

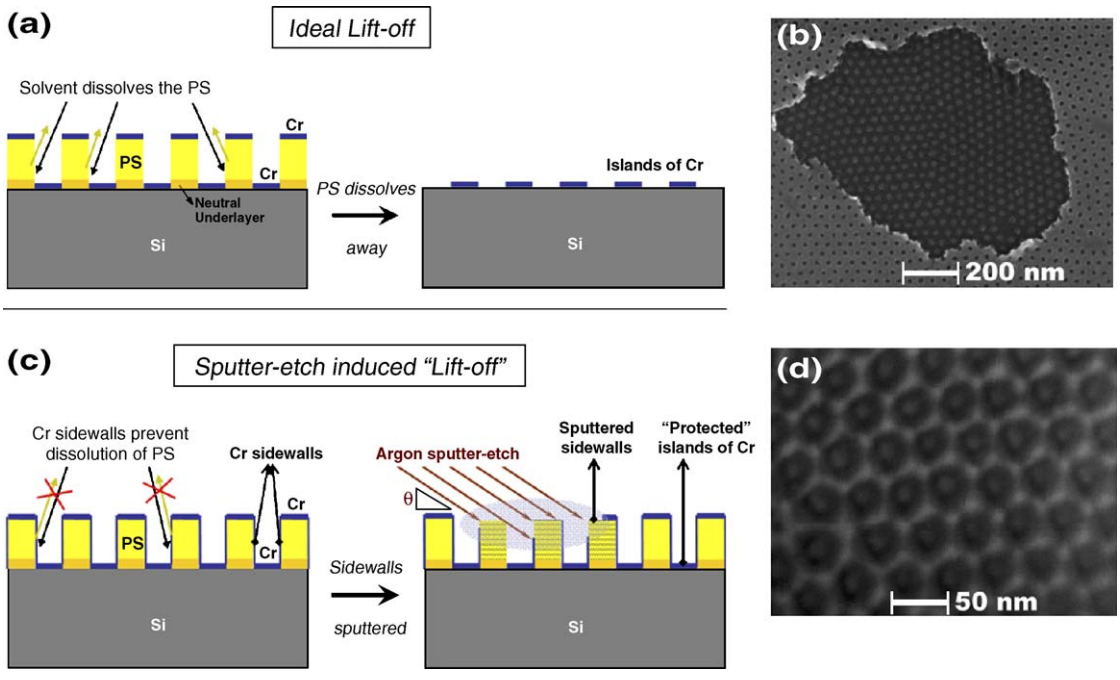

Fig. 1. Schematic and pictures of different types of lift-off. (a) Ideal lift-off: in the ideal scenario, the metal (Cr) layer forms only on top of the template and on the exposed substrate (Si). The solvent dissolves away the template (PS), "lifting-off" the unwanted Cr, and leaving the Cr islands on the substrate. (b) SEM of a region of successful lift-off — in our samples these regions were typically smaller than a few microns. (c) Sputter-etch induced "lift-off": During metal evaporation, a thin coating of Cr forms on the template sidewalls, preventing dissolution of the template. Oblique-angled Ar ions are used to sputter-etch the template over cm-sized areas. (d) SEM of template after the Ar sputter-etch step. The hexagonal sidewalls of the template disintegrate during the RIE, while the inner Cr islands hold up and yield nanopillars.

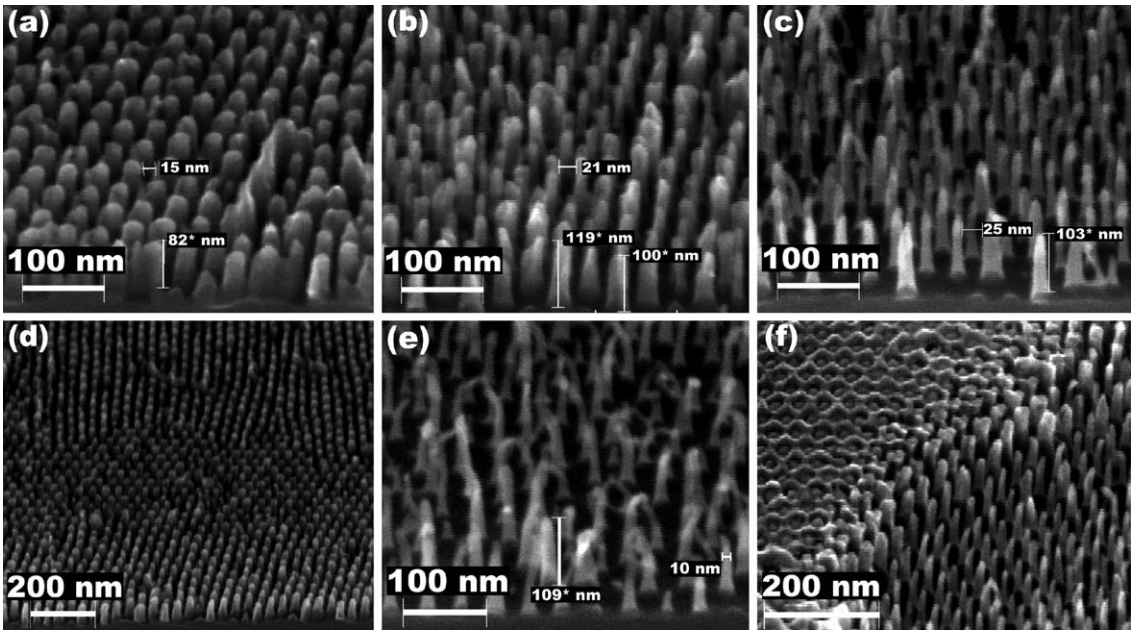

Fig. 2. SEM images of nanopillars in Si under different conditions. Using 5 nm of Cr as the etch-mask, and after sputter-etching with Ar for 10 min, nanopillars of Si are formed after (a) 4 min (b) 5.5 min and (c) 7 min of NF_3 RIE. (d) An example of the large-area coverage of the nanopillars. (e) Nanopillars distort when the aspect-ratio becomes very high (>8 : 1). (f) A micrograph showing the difference between RIE etched and unetched regions (a dust particle probably shadowed the RIE in the upper-left-corner unetched region). In the unetched region the hexagonal pattern subsequent to the Ar sputter-etch step is clearly seen. * indicates dimensions that have been corrected for the imaging angle (45° tilt).

masks. The duration of Ar sputter-etching was critical and needed to be optimized (as discussed in a later section). The hexagonal sidewalls were not removed cleanly by the sputter-etch (Fig. 1d). Close inspection of this figure also revealed the directionality of the sputter-etch — the Ar ions approached from the lower-left and the presence of what appears to be a "shadow" (not an SEM imaging artifact) in the lower left regions of the hexagonal artifacts indicates slightly different effects of the sputter-etching in different directions around the pore. Nevertheless, such a directional sputter-etch is sufficient for the purposes of this work as evidenced by the final nanopillar structures. After the sputter-etch, the samples were soaked in different solvents (toluene, acetone, chloroform) for up to 24 h and the sidewalls were still not lifted-off. We concluded that the sputter-etching had etched away the Cr from the tops of the sidewalls, but had left behind sidewalls that were a mixture of insoluble PS and tiny particles of "knocked-in" Cr.

Since PS does not stand up to the NF_3 based RIE [19] used to etch Si, we could etch the desired pattern into Si. The hexagonal walls around the Cr islands were not resistant to the etch conditions and disintegrated, whereas the Cr islands themselves were remarkably resistant and yielded Si nanopillars. NF_3 has been known to etch polymers, such as Novolac-based positive photoresists, with an etch-rate of ca. 25 nm/min. It has also been used as a clean-up gas to remove polymer debris formed during RIE of SiO_2. NF_3 produces free F that converts organic material into volatile CF_4 and Si into volatile fluorides; Cr, however, is not converted into a volatile product. The PS in the sidewalls is etched away by the NF_3, while the tiny Cr particles within the sidewalls are removed during the decomposition of the PS into volatile fragments. The Si etch-rate to Cr etch-rate ratio was greater than 20 : 1, even at this 50 nm patterning lengthscale. The anisotropic feature of the etching conditions produced vertical nanopillars with dimensions that depended on both the Ar sputter-etch time and the RIE time. Representative SEM micrographs of such structures are shown in Fig. 2. Table 1 summarizes the nanopillar feature sizes under different processing conditions.

It is believed that the presence of nitrogen in NF_3 serves to passivate the sidewalls of the pillars during etching enabling the anisotropic structures. Other fluorine based RIEs are not as effective in obtaining such structures; SF_6 is plagued by an unacceptable level of undercutting, whilst CF_4 does not provide enough anisotropy. Chlorine and HBr based RIE at low chamber pressures is one possible alternative although excessive sidewall deposition during the process could prove cumbersome. Besides fulfilling the main goal of achieving the nanostructures, NF_3 also removes the insoluble PS sidewalls. Nevertheless, it is not inconceivable that a combination of more common etch chemistries will be able to achieve these results.

Table 1
A summary of the nanopillar dimensions with different sputter-etch and RIE times

NF_3 etch times	10 min Ar sputter-etch		12 min Ar sputter-etch	
	Height (nm)	Width (nm)	Height (nm)	Width (nm)
4 min	82	20	63	20
5.5 min	106	18	88	16
7 min	99	12	106	10
8 min	56	8	0	0

Tilt during imaging has been accounted for in these dimensions.

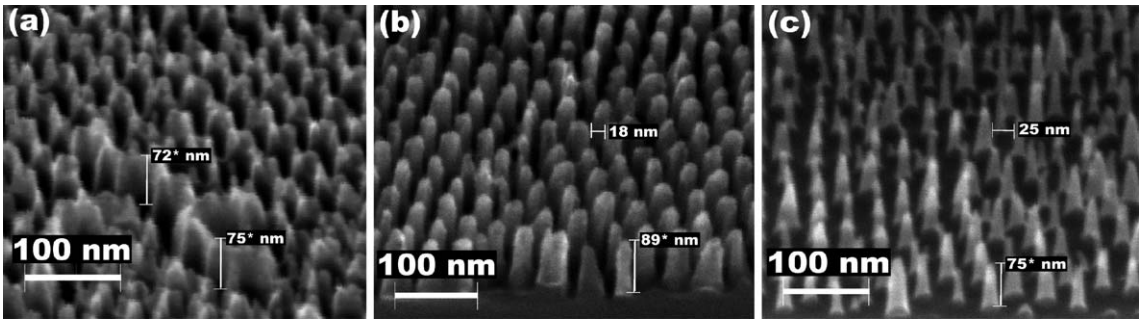

Fig. 3. Ar sputter-etch time is critical for obtaining good nanopillars. (a) An insufficient Ar sputter-etch leads to convoluted sidewalls and nanopillars as the final nanostructure. (b) Optimum time of Ar sputter-etching leads to optimum nanopillars. (c) Excessive Ar sputter-etching leads to insufficient Cr remaining on the Si and consequently narrower and shorter pillars.* indicates dimensions that have been corrected for the imaging angle (45° tilt).

Various unique aspects of the materials and processing techniques enabled key features of the nanostructures. Firstly, nanopillars with periodicities of less than 35 nm were afforded by the RIE of the densely packed array of Cr islands patterned by BCP lithography. It may be noted that the periodicity of the self-assembled film increases with the molecular weight of the BCP as does the pillar diameter; the reported range of periodicities in this BCP system is about 25 to 80 nm [8]. Secondly, BCP lithography facilitates the well-ordered arrangement of the nanopillars. Optimum spin-coating and annealing conditions produce ordered arrays of pores in a hexagonal matrix that are defect-free over hundreds of nm. Allowing for a few defects and grain-boundaries, order can therefore be achieved over millimeters. Thirdly, the unique Ar sputter-etch technique reported in this work enables, in principle, a limitless extent of effective lift-off. We have demonstrated lift-off and fabrication of nanopillars over cm-sized areas — $(0.5\,\mathrm{cm})^2$ to $(1\,\mathrm{cm})^2$. Finally, it is the highly selective and anisotropic nature of the RIE chemistry involving NF_3 that makes possible the fabrication of tall, vertical nanopillars despite having only 5 nm of Cr etch-mask — nanopillars taller than 100 nm and having aspect-ratios as high as 10 : 1 were created.

We believe that these processing conditions may be suitably extended to many other BCP template systems. For instance, with the polystyrene-polyisoprene approach to nanopatterning [10], a combination of Cr deposition and oblique-angled sputter-etching could yield a large-area nano-dot pattern. For that matter, the sputter-etching technique for effective lift-off should find application with any BCP system in which one of the blocks can be selectively removed, eventually leading to a thickness contrast (of polymer) on the substrate. The technique will be especially useful when this thickness contrast is between 15 and 30 nm and conventional means of lift-off are ineffective. An increasingly glancing angle of sputter-etching is recommended for small thickness contrasts. The sputter-etching technique may also be extended to BCP templates that have patterns different from the hexagonal arrangement described in this work. For example, BCP templates of parallel stripes may be subjected to metal deposition and lift-off via sputter-etching to obtain the pattern in metal; the direction of the sputter-etch should be as perpendicular to the stripes as possible to keep the metal on the substrate sheltered from the sputtering ions. The NF_3 RIE is most effective when etching Si with Cr as the etch-mask, which may be present in different patterning geometries; Cr deposition and lift-off via sputter-etching could facilitate just this using various BCP systems. This RIE may be directly applied to BCP systems that incorporate Cr into one of the organometallic blocks (similar to BCP systems in [11,12]). For etching materials besides Si, suitably selective etch-chemistries will need to be developed; the sputter-etch lift-off technique, however, should still prove useful in producing a metal etch-mask if needed.

We observed that an optimum duration of the sputter-etching was vital for obtaining good nanopillars. Fig. 3a–c depicts different structures obtained with different times of sputter-etching. Too short a time of sputter-etching did not sputter enough Cr off the sidewall tops, which led to some parts of the sidewalls being resistant to the RIE. The resulting nanostructure consisted of a convoluted pattern of pillars and interconnecting ridges (Fig. 3a). When the sample was sputter-etched for too long, the Cr from the sidewall tops was sufficiently removed. However, the hitherto "protected" Cr islands on the Si also appear to have been etched. Thus, the effective thickness and diameter of the Cr-etch-mask was compromised, and as a result, the diameter of the nanopillars was smaller and the maximum pillar-height obtainable was reduced (Fig. 3c). The sputter-etch time was optimized by making samples with varying sputter-etch times, correlating nanostructures obtained after RIE with the corresponding sputter-etch times and selecting the conditions that yielded the best results (Fig. 3b).

The structure of the nanopillars – shape, height and diameter – were also shown to depend on the different times of Ar sputter-etching and NF_3 RIE. Table 1 summarizes some of the most relevant data for two cases — a 10-min Ar sputter-etch, which gave the best nanopillars, and a 12-min Ar sputter-etch. For the 10-min Ar-sputter-etch case, as the NF_3 etch times increased from 4 to 5.5 min the nanopillars grew taller and thinner. Beyond 5.5 min, the Cr barrier atop the pillars is etched away and the tops of the pillars begin to get etched. This, coupled with the progressive thinning of the nanopillars, causes the nanopillar heights to actually decrease on further etching. For the 12-min Ar-sputter-etch case, a similar trend is seen and after 8 min of NF_3 etch, there remained only stubby

vestiges of what were once pillars because of an insufficient Cr etch barrier. Using these strategies, nanopillars ranging from 80 to 110 nm in height were engineered. Achieving shorter nanopillars should be possible by shortening the RIE time. Interestingly, nanopillars taller than ca. 110 nm showed signs of distortion when their diameters shrank below 10 nm. The reason for the mechanically unstable nanopillars is unclear, but it could be due to a slight undercutting of the stem of the pillar leading to a "bulb" of Si (just beneath the Cr) to be supported by a slim neck. Therefore, the height of the nanopillars appears to be limited by a combination of their aspect ratio and absolute diameter. Obtaining taller nanopillars would require starting with larger (in diameter) and possibly thicker Cr islands. Straight pillars over 600 nm tall with diameters larger than 50 nm, fabricated using electron-beam lithography and the same NF_3 RIE chemistry, have been reported [19].

The surface properties of the nanopillars could be important for many applications. In bulk-heterojunction photovoltaic cells, for instance, electron transfer between the Si and the other semiconductor will be affected, either adversely or constructively, by the nature of the surface. XPS was used to analyze the surface of the nanopillars and Table 2 summarizes the chemical compositions of the sample at various stages of processing. Immediately after the NF_3 etch, the surface of the Si nanopillars contains a fair amount of the Si present as an oxide. The surface also had many contaminants composed of C, N, F (presumably from the etching environment), and Cr (remnants of the etch-mask). It was found that 60 min of UV-ozone treatment followed by rinsing in dilute hydrofluoric (HF) acid for approximately 15 min yielded clean pillars (with only trace impurities). At this stage, we believe that the surface of the nanopillars is pristine, H-passivated Si, because the Si XPS signal indicates a single chemical state (pure Si or Si–H, which cannot be distinguished by XPS) and because when placed in air the Si surface does not oxidize for at least a couple of hours after the HF strip. The Si can be subsequently treated in suitable ways to achieve the required surface properties. SEM micrographs show that the structure of the nanopillars does not appear altered in any significant manner after the UV-ozone and HF-stripping treatments.

Table 2
A summary of the chemical composition of the nanopillar surface after various treatments

Element details	NF_3 (3 min)		
		UVO (60 min)	UVO (60 min)
			HF (13 min)
Si	14%	32%	94%
(% as Si)	(73%)	(49%)	(100%)
(% as oxide)	(27%)	(51%)	
O	20%	52%	3.4%
Cr	1.8%	3.5%	
F	24%	3.1%	2.1%
N	9%	4.1%	
C	32%	4.5%	

Percentages above 5 are rounded to the nearest percent and those under 5 are rounded to the nearest tenth of a percent, as this best represents the accuracy of the measurements.

4. Conclusions

We have described a procedure to obtain densely packed, well-ordered, high-aspect-ratio Si nanopillars covering large substrate areas. It was found that different processing conditions had a dramatic effect on the final nanopillar structure and surface chemistry. Block copolymer lithography is a versatile technique for creating BCP templates on different substrates with different geometries at a sub-100 nm lengthscale. A unique lift-off technique for overcoming prohibitive etch-mask lift-off problems has been demonstrated, which could have significant application with many BCP templates (thereby extending their potential) and other lithographic processes, especially at the nanometer lengthscale. We have also showcased an enabling RIE chemistry — high-aspect-ratio nanostructures in other materials could be obtained by employing a suitably selective and anisotropic RIE chemistry.

References

[1] J.J.M. Halls, C.A. Walsh, N.C. Greenham, E.A. Marseglia, R.H. Friend, S.C. Moratti, A.B. Holmes, Nature 376 (1995) 498.
[2] K.M. Coakley, M.D. McGehee, Chem. Mater. 16 (2004) 4533.
[3] S.G. Johnson, S.H. Fan, P.R. Villeneuve, J.D. Joannopoulos, L.A. Kolodziejski, Phys. Rev., B Condens. Matter (USA) 60 (1999) 5751.
[4] T.H. Martin Kamp, Sven Mahnkopf, Alfred Forchel, Srinivasan Anand, Guang-Hua Duan, in: S.L. Kurt Busch, Ralf B. Wehrspohn, Helmut Foll (Eds.), Photonic Crystals: Advances in Design, Fabrication, and Characterization, John Wiley & Sons, 2004, p. 329.
[5] H.T. Ng, J. Han, T. Yamada, P. Nguyen, Y.P. Chen, M. Meyyappan, Nano Lett. 4 (2004) 1247.
[6] K. Shin, K.A. Leach, J.T. Goldbach, D.H. Kim, J.Y. Jho, M. Tuominen, C.J. Hawker, T.P. Russell, Nano Lett. 2 (2002) 933.
[7] D.H. Kim, X.Q. Jia, Z.Q. Lin, K.W. Guarini, T.P. Russell, Adv. Mater. 16 (2004) 702.
[8] K.W. Guarini, C.T. Black, K.R. Milkove, R.L. Sandstrom, J. Vac. Sci. Technol., B 19 (2001) 2784.
[9] C. Harrison, M. Park, P.M. Chaikin, R.A. Register, D.H. Adamson, J. Vac. Sci. Technol., B 16 (1998) 544.
[10] R.R. Li, P.D. Dapkus, M.E. Thompson, W.G. Jeong, C. Harrison, P.M. Chaikin, R.A. Register, D.H. Adamson, Appl. Phys. Lett. (USA) 76 (2000) 1689.
[11] J.Y. Cheng, C.A. Ross, V.Z.H. Chan, E.L. Thomas, R.G.H. Lammertink, G.J. Vancso, Adv. Mater. 13 (2001) 1174.
[12] J.Y. Cheng, C.A. Ross, E.L. Thomas, H.I. Smith, G.J. Vancso, Appl. Phys. Lett. (USA) 81 (2002) 3657.
[13] K. Temple, K. Kulbaba, K.N. Power-Billard, I. Manners, K.A. Leach, T. Xu, T.P. Russell, C.J. Hawker, Adv. Mater. 15 (2003) 297.
[14] C.T. Black, K.W. Guarini, K.R. Milkove, S.M. Baker, T.P. Russell, M.T. Tuominen, Appl. Phys. Lett. (USA) 79 (2001) 409.
[15] K. Liu, S.M. Baker, M. Tuominen, T.P. Russell, I.K. Schuller, Phys. Rev., B Condens. Matter (USA) 63 (2001) 403.
[16] K.W. Guarini, C.T. Black, Y. Zhang, H. Kim, E.M. Sikorski, I.V. Babich, J. Vac. Sci. Technol., B 20 (2002) 2788.
[17] E. Huang, S. Pruzinsky, T.P. Russell, J. Mays, C.J. Hawker, Macromolecules 32 (1999) 5299.
[18] E. Huang, T.P. Russell, C. Harrison, P.M. Chaikin, R.A. Register, C.J. Hawker, J. Mays, Macromolecules 31 (1998) 7641.
[19] H. I.-H. Liu, Ph.D. Thesis ("Fabrication and Properties of Silicon Nanostructures"), Department of Electrical Engineering, Stanford University, CA, USA, 1995.